# [B10H10]2– Nanoclusters Covalently-Immobilized to Hybrid SiO2 Aerogels for Slow Neutron Shielding Applications

**Article** · August 2022

DOI: 10.1021/acsanm.2c02550



**12 authors**, including:

Khursand E. Yorov
King Abdullah University of Science and Technology


Alexander E. Baranchikov
Russian Academy of Sciences


G. P. Kopitsa
Petersburg Nuclear Physics Institute


Oleg I. Pokrovskiy
Russian Academy of Sciences

# $[B_{10}H_{10}]^{2-}$ Nanoclusters Covalently-Immobilized to Hybrid $SiO_2$ Aerogels for Slow Neutron Shielding Applications

*Khursand E. Yorov[1], Andrey P. Zhdanov[1], Rustam Kh. Kamilov[2], Alexander E. Baranchikov[1], Gennady P. Kopitsa[3], Oleg I. Pokrovskiy[1], Anton L. Popov[4], Olga S. Ivanova[1], László Almásy[5], Yury G. Kolyagin[2], Konstantin Yu. Zhizhin[1], Vladimir K. Ivanov[1,6]**

[1]Kurnakov Institute of General and Inorganic Chemistry, Russian Academy of Sciences, Leninsky prosp. 31, Moscow 119991, Russia

[2]Lomonosov Moscow State University, Leninskie Gory 1, Moscow 119991, Russia

[3]Petersburg Nuclear Physics Institute of National Research Centre "Kurchatov Institute", Orlova Roscha 1, Gatchina 188300, Russia

[4]Institute of Theoretical and Experimental Biophysics, Russian Academy of Sciences, Institutskaya ul. 3, Pushchino 142290, Russia

[5]Institute for Energy Security and Environmental Safety, Centre for Energy Research, 1121 Budapest, Konkoly Thege Miklós út 29-33, Hungary

[6]National Research University Higher School of Economics, Pokrovskiy blvd. 11, Moscow 109028, Russia

radiation resistance; safety; silanes; decaborate; boron; sol-gel; electrophilic induced nucleophilic substitution

An alkoxysilane derivative bearing 10-vertex *closo*-decaborate nanocluster ($B_{10}H_{10}^{2-}$) was successfully synthesized and immobilized in $SiO_2$ aerogel matrix. *closo*-Decaborate-containing $SiO_2$ aerogels showed high specific surface (~750 $m^2$/g), open porosity (~95 %) and extremely low apparent density (80 mg/$cm^3$) as well as increased thermal stability of *closo*-decaborate moiety. Despite the low boron content (~1.2 mol.% of boron nanoclusters comprising natural mixture of boron isotopes), the aerogel nanomaterial demonstrated excellent neutron capture properties exceeding lightweight polymer-based analogues. Cell viability assessment indicated the pronounced dose-dependent toxicity of borylated aerogel with respect to malignant cells (U251 MG glioblastoma line), and low toxicity with respect to normal cells (dental pump stem cells). The combination of the properties of *closo*-decaborate modified silica aerogels make them good candidate material for shielding of patients and healthcare personnel during boron neutron capture therapy procedures.

## 1. Introduction

Most recently, advances in the use of new neutron sources for neutron activation analysis, neutron radiography, active neutron interrogation technique, and neutron capture therapy emerged an interest in neutron-shielding materials.[1,2] Neutron-shielding materials are intended to neutralize unwanted neutron radiation, which otherwise could result in radioactive contamination of the environment or excessive human radiation exposure. In the shielding from high-energy neutrons (more than 2 MeV), concrete- or metal-based composite materials are generally used containing hydrogen-rich neutron moderators (water or organic polymers) and slow neutron absorbers. Among slow neutron absorbers, boron compounds are preferable due to the extremely high $^{10}B$ neutron cross-section (3 837 barns) and high $^{10}B$ content in natural boron (~20 %).[3,4]

In concrete- or metal-based neutron shields, high-energy neutrons can interact with heavy atoms resulting in high secondary radiation, thus hydrogen-rich polymer-based boron-containing composites are now commonly preferred (*e.g.* high-density polyethylene, ultrahigh molecular weight polyethylene, polyvinyl alcohol, epoxy resins, ethylene propylene diene monomer rubbers, styrene-butadiene rubbers, silicon rubbers)[1]. Moreover, the most attractive feature of polymer-based composites is their relative low density that is inaccessible in concretes or metals, which makes them material of choice for the personnel safety wears. In boron neutron capture therapy, low-energy (<0.5 eV) thermal neutrons are used, thus in personnel safety wear no heavy elements are required and so the materials containing only hydrogen-rich neutron moderator compounds and boron atoms are appropriate.[1,2]

One of the important characteristics of the neutron-shielding materials is their radiation resistance. Generally, polymer neutron absorbing materials are vulnerable to irradiation damage.[5] With the increase in the irradiation dosage, polymer-based materials undergo chemical and structural transformations resulting in reducing the molecular weight, emission of various gases (including CO, $CH_4$) which lead to the formation of voids in the polymer matrix reducing its mechanical strength and shielding efficiency.[5] The weight of the neutron capturing materials is another parameter of primary importance for the protection of oncology patients during boron neutron capture therapy. Despite the relatively light weight of polymer materials, they possess typical density of around 1 g/cm$^3$,[6] which gives more than 2 kg per single borylated polymer slab in a typical therapeutical procedure.[7] Any possible decrease in the weight of the shielding cover is preferable to provide minimum discomfort to the persons with heavily impaired health.

Aerogels can be regarded as alternative candidate materials for neutron-shielding applications, as they combine ultra lightweight and highly developed open porosity which ensures free removal of any gaseous products formed upon neutron irradiation.[8] To create highly efficient neutron absorbers, boron atoms should be incorporated into aerogel nanomaterials. The literature survey shows that up to now, only a single attempt to produce aerogel-like neutron-shields was reported.[9] The highly porous boron containing alginate materials were obtained using a freeze-drying technique (thus, in a strict sense they cannot be regarded as aerogels) and showed high neutron absorption efficiency (93–99 %) and low density (nearly 100 mg/cm$^3$). The synthesis of the materials was based on a simple mixing of boron-containing microparticles ($B_4C$, BN and/or zinc borate) and montmorillonite with sodium alginate aqueous solution. Such an approach cannot guarantee the homogeneous distribution of microparticles within the matrix, thus high boron loading was necessary for the production of efficient shielding materials, the content of boron-containing compounds reached ~47 wt.% to achieve 99.1 % neutron absorption efficiency.

The scantiness of the reports on the aerogels for neutron shielding applications is connected obviously to the synthetic limitations. The reported methods for the incorporation of boron into lightweight materials are based on the simple mixing of the matrix with microparticles of boron-containing compounds, *e.g.* $B_4C$, BN, zinc borates, boric acid.[5,10,11] Similar methods are hardly suitable to produce aerogel materials as microparticles will tend to sediment during the sol-gel transition stage of the aerogels synthesis. The segregation of the material components will impair its protective property.

Thus, a brand new strategy is required to produce neutron-shielding aerogels for the patients' protection in neutron capture therapy. The strategy should include the proper choice of aerogel matrix, and the method for the incorporation of boron in the matrix, ensuring homogeneous distribution of boron in the material during the sol-gel transition. The design of new ultralight materials bearing high neutron capture cross-section elements (*e.g.* boron) can open new diverse applications, from neutron-shields to boron neutron capture therapy to new neutron detectors.[12]

Recently, numerous successful attempts were reported on the synthesis of silica aerogels immobilized with various coordination compounds, the methods for their synthesis are based on the gelation of pre-constructed hybrid silanes with particular functional moieties.[13] Generally, organosilanes due to their unique chemical flexibility are commonly respected for the synthesis of hybrid functional aerogels.[14–17] Being one of the bright examples of advanced nanomaterials, silica aerogels are non-toxic and biocompatible, they contain high amount of hydrogen (as water molecules, surface hydroxyl groups and low molecular weight organic moieties) which is an effective neutron moderator. On the other hand, their extended surface provide effective scattering of thermalized neutrons that can further be captured by boron atoms with high neutron capture cross-section.

Wide opportunities to link various organic, organoelement or coordination moieties to silica matrix make it possible to chemically immobilise boron in $SiO_2$ aerogels. The survey in boron chemistry makes cluster boron anions $[B_nH_n]^{2-}$ ($n$ = 10, 12) as the moieties of choice to produce such hybrid materials. Over decades, a constant interest to the compounds bearing such clusters originates from the wide range of their applications, high chemical and thermal stability which is due to 3D aromaticity.[18] On the other hand, electron deficient nature of the clusters make them susceptible to various substitution reactions, which allows for the molecular design through their decoration with different functional groups.[19–22] Functionalized *closo*-borates are used to create energy storage materials and fuels,[23–25] components of non-linear optic systems,[26,27] catalysts,[28,29] molecular magnetics,[30,31] *etc.* High specific boron content in the compounds bearing $[B_nH_n]^{2-}$ clusters is the main concern for the consideration for substituted *closo*-borates for boron neutron capture therapy.[32–37]

The most convenient synthetic approach for the chemical modification of *closo*-borate anions (*e.g.* $[B_{10}H_{10}]^{2-}$) is based on electrophilic induced nucleophilic substitution (EINS) reactions.[38] This approach allows appending various functional groups to *closo*-decaborate moiety, which can further be chemically modified, *e.g.* with cyclic oxonium or nitrilium groups.[39,40] For example, nucleophilic addition to multiple bond of nitrilium derivatives and cycloaddition reactions makes it possible to synthesize *closo*-decaborates with a wide range of functionalities.[40–42] The synthesis of functionalized $[B_{10}H_{10}]^{2-}$ anions is also very attractive for their further immobilization on the carriers' surface.[43–45]

Functional groups (X) are typically immobilized on the surface of silica matrix by using substituted alkoxy silanes bearing a $–(CH_2)_n–$ linker, $(RO)_3Si(CH_2)_nX$.[46,47] According to this approach, to provide chemical bonding of *closo*-decaborate cage $[B_{10}H_{10}]^{2–}$ to $SiO_2$ matrix, alkoxy silylated *closo*-decaborate clusters ($(RO)_3Si–(CH_2)_n–B_{10}H_9$) are the best candidates. Up to now, the synthesis of alkoxy silane derivatives of *closo*-decaborates has not been virtually reported. To the best of our knowledge, the only available example was provided by Abi-Ghaida *et al.*[43] In their study, the first trialkoxy silyl substituted *closo*-decaborate clusters were synthesized, $[2\text{-}B_{10}H_9NC(CH_2)_3Si(OC_2H_5)_3]^–$ and $[1\text{-}B_{10}H_9NH_2CH_2CH_2NHCONH(CH_2)_3Si(OC_2H_5)_3]^–$. These clusters were successfully immobilized on the surface of mesoporous silica (SBA-15). The further research of Abi-Ghaida *et al.*[44] was focused on the immobilization of alkoxy silylated *closo*-decaborates on the surface of Stöber silica. Any reports on the chemical immobilization of boron clusters in $SiO_2$ aerogels have not been presented yet.

In this study, we report the preparation of a new triethoxy-silylated *closo*-decaborate cluster and its immobilization onto a silica aerogel through co-condensation with a silicon alkoxide. During the aerogel synthesis, the *closo*-decaborate moiety remained intact; the resultant hybrid material possessed high specific surface and porosity inherent in nanostructured aerogel materials. High neutron capture characteristics as well as extremely low apparent density make the material suitable for the design of ultralight weight neutron shielding covers for the patients and healthcare personnel during boron neutron capture therapy procedures.

## 2. Experimental Section

### *2.1 Materials*

The following reagents were used as starting materials: (3-aminopropyl)triethoxysilane (APTES, 99 %, Aldrich), tetraethoxysilane $Si(OC_2H_5)_4$ (TEOS, 99 %, Aldrich), methyl alcohol (MeOH, 99.5+ %, Acros), acetonitrile (MeCN, high-grade, Khimmed), triethylamine ($NEt_3$, 99 %, Acros), decaborane(14) (20 % toluene solution, JSC Aviabor), $CF_3COOH$ (99 %, Sigma-Aldrich), $CH_3COOH$ (glacial, ≥99 %, Sigma-Aldrich), isopropanol (high-grade, Khimmed), HCl (0.1 M, aqueous solution, prepared from 37 % analytical grade aqueous solution, Khimmed), $NH_3{\cdot}H_2O$ (0.833 M, aqueous solution, prepared from 25 % analytical grade aqueous solution, Khimmed), dichloromethane (≥99.9 %, Sigma-Aldrich), diethyl ether (≥99.0 %, Sigma-Aldrich) and distilled water. The decaborane(14) was used as received, no isotopic enrichment procedures were applied. The synthesis of $(^nBu_4N)_2[B_{10}H_{10}]$ was conducted *via* the intermediate 1,6-bis(triethylamine)decaborane according to the previously reported protocol.[48] Tetra-*n*-butylammonium 2-acetonitrilium-*closo*-decaborate $(^nBu_4N)[2\text{-}B_{10}H_9NCCH_3]$ (**CNB**) was prepared according to the previously reported procedure.[49] All solvents were purified according to the conventional methods.[50]

### *2.2 Synthesis of* APTES-B

To the solution of **CNB** (2.01 g, 5.0 mmol) in dichloromethane (20 mL) (3-aminopropyl)triethoxysilane (APTES) (2.34 mL, 10.0 mmol) was added. The reaction mixture was stirred under argon atmosphere at room temperature for 3 hours. Then solution was evaporated and solid residue was recrystallized from $CH_2Cl_2$ / petroleum ether. The solid product was dried over $P_4O_{10}$. The yield was 2.68 g of **APTES-B** (85.7 %). $^1H$ NMR (δ): 8.41 (s, br, 1H N**H**-$CH_2$), 5.73 (s, br, 1H N**H**=C), 3.83 (q, 6H, OC**$H_2$**$CH_3$, 7 Hz), 3.16 (8H, $NBu_4^+$), 2.62 (t, 2H, C**$H_2$**$CH_2CH_2Si$, J =7 Hz), 1.98 (s, 3H, C-C**$H_3$**), 1.79 (m, 2H, $CH_2C$**$H_2$**$CH_2Si$), 1.59 (8H, $NBu_4^+$), 1.41 (8H, $NBu_4^+$), 1.22 (t, 9H, $OCH_2C$**$H_3$**, J = 8 Hz), 1.01 (12H, $NBu_4^+$), 0.74 (t, 2H, $CH_2CH_2C$**$H_2$**Si, J = 8 Hz), 1.75 to -0.66 (m, 9H, BH). $^{11}B$ NMR (δ): 3.5 (d, 1B, B(10), $J^1_{BH}$ = 146 Hz), –3.7 (d, 1B, B(1), $J^1_{BH}$ = 142 Hz), –14.5 (s, 1B, B(2)), –23.3 (d, 4B, B(3,5)+B(6,9), $J^1_{BH}$ = 105 Hz), –26.3 (d, 3B, B(4)+B(7,8), $J^1_{BH}$ = 110 Hz). $^{13}C$ NMR (δ): 165.1 (N=**C**$CH_3$), 59.6 ($NBu_4^+$), 59.1 (O**C**$H_2CH_3$), 46.7 (**C**$H_2CH_2CH_2Si$), 24.8 ($NBu_4^+$), 24.1 (N=C**C**$H_3$), 20.5 ($NBu_4^+$), 20.1 ($CH_2$**C**$H_2CH_2Si$), 18.9 ($OCH_2$**C**$H_3$), 14.2 ($NBu_4^+$),8.2 ($CH_2CH_2$**C**$H_2Si$). IR (KBr, $cm^{-1}$, selected bands): ν(NH) 3338, 3313, 3267; ν(CH) 2968, 2934, 2877; ν(BH) 2477, ν(C=N) 1648. δ(B-B-H) 1079. $ESI^-$-MS (*m/z*): 379.50 ($[A]^-$, calc. 379.60). Calc. for $C_{27}H_7B_{10}N_3O_3Si$, (623.6): C, 51.95; H, 11.47; N, 6.74; B, 17.7. Found: C, 52.06; H, 11.44; N, 6.70; B, 17.5.

### *2.3 Synthesis of hybrid lyogels*

For the synthesis of hybrid silica lyogels, a two-stage sol-gel method was used. At the first stage, tetraethoxysilane (TEOS) was hydrolysed by the addition of 3.39 mL of $7.5 \cdot 10^{-3}$ M hydrochloric acid (pH 2.1) to a solution of TEOS (14.00 mL, 62.7 mmol) in methanol (7.61 mL), with vigorous stirring. Before the lyogel synthesis, the resulting transparent sol was aged for 24 h. In a separate container, 0.607 g ($1.06 \cdot 10^{-3}$ mol) of **APTES-B** was dissolved in a mixture of 68 mL $CH_3OH$ and 50 mL $CH_3CN$. 25 mL of $SiO_2$ sol was added to **APTES-B** solution for co-gelation. For the synthesis of bare $SiO_2$ lyogel, 25 mL of $SiO_2$ sol was added to a solution comprising 50 mL $CH_3OH$, 68 mL $CH_3CN$ and 15 mL of 0.83 M aqueous ammonia. The following designation of the samples is further used in the manuscript: **$SiO_2$** (pure $SiO_2$ aerogel), **$SiO_2$–B** ($SiO_2$ aerogel modified with **APTES-B**). Fig. 1 shows the scheme for the **APTES-B** and **$SiO_2$–B** synthesis.

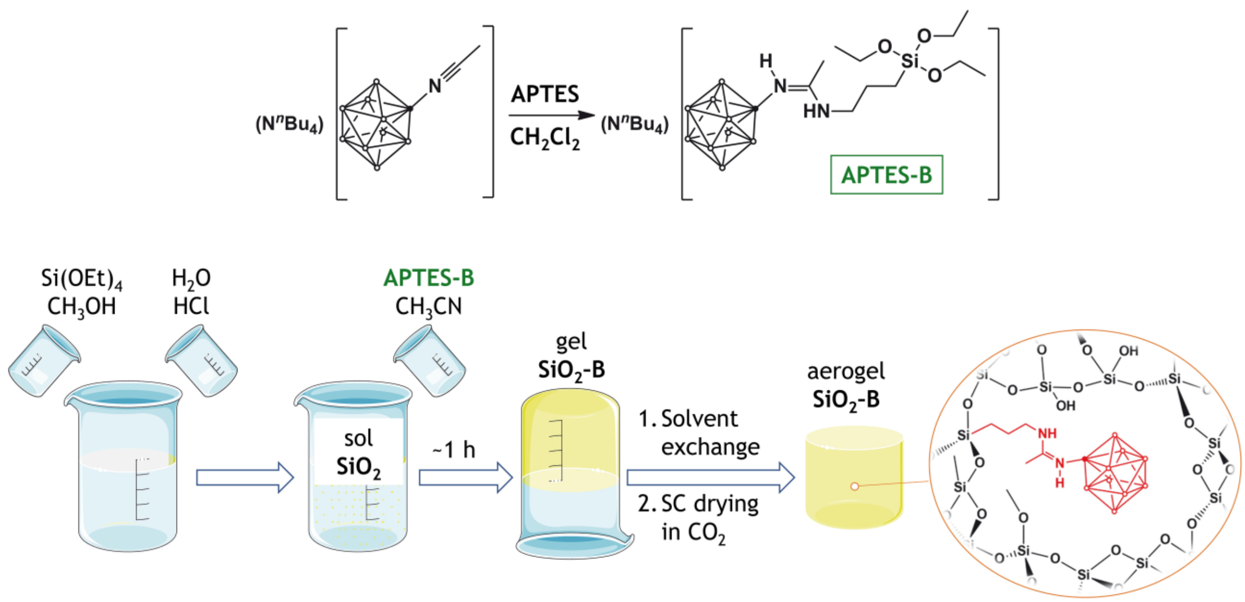


**Figure 1.** The synthesis scheme for the **APTES-B** silylated *closo*-borate and **$SiO_2$–B** aerogel.

The lyogels were aged for 4 days, then they were washed with isopropanol once a day for 5 days. The washing solutions were collected for further analysis of **APTES-B** content. Next, lyogels were dried under supercritical $CO_2$.

### *2.4 Supercritical drying of lyogels*

For the synthesis of aerogels, lyogels were dried in supercritical $CO_2$. Supercritical drying in $CO_2$ (critical parameters: $t_c$ = 31 °C, $P_c$ = 72.8 atm) was conducted using a setup comprising a high-pressure pump, Supercritical 24 (SSI, USA), a 50 mL steel reactor and a back pressure regulator BPR (Goregulator, Waters, USA). Lyogel samples were washed with liquid $CO_2$ for 2 h at 20 °C and 150 atm, then the temperature in the reactor was raised to 50 °C and the samples were washed for 2.5 hours with supercritical $CO_2$ at 120 atm. Then, the pressure in the heated autoclave was gradually (within 30–40 minutes) reduced to atmospheric pressure, the autoclave was cooled down and opened.

### *2.5 Physical characterization*

NMR ($^1$H, $^{11}$B, $^{13}$C) spectra of the studied compounds were recorded on a Bruker AVANCE II 300 spectrometer operating at 300.3, 96.32 and 75.49 MHz, respectively, using internal deuterium lock. To perform the measurements, the samples were dissolved in $CD_2Cl_2$. Tetramethylsilane and boron trifluoride etherate were used as external references.

$^{11}$B MAS NMR experiments were performed on a Bruker AVANCE II 400 spectrometer (9.4T, $\nu$($^{11}$B) – 128.37 MHz). For recording $^{11}$B MAS NMR spectra, 4 mm HX MAS probe with spinning rate of 12 kHz was used. $^{11}$B MAS NMR spectra were recorded with 15-degree pulse length of 0.8 µs, a recycle delay of 0.5 s and for 4096 scans. The chemical shifts were referenced to $BF_3{\cdot}Et_2O$ (0 ppm).

Electrospray Ionisation Mass Spectrometry (ESI MS) for the solutions of the compounds in MeCN were recorded on a Bruker Daltonik MicrOTOF-Q spectrometer. Apollo II was used as an electrospray ionization source, ion spray voltage ±4.5 kV, $t$ = 200°C, flow rate 3 µL/min. Analysis was conducted at the IREA Shared Analytical Facilities Center of the National Research Center "Kurchatov Institute".

The IR spectra of the samples were recorded using the attenuated total internal reflection technique (ATR) in the range of 400–4000 cm$^{-1}$ on a Perkin Elmer Spectrum 65 spectrophotometer equipped with a Quest ATR Accessory (Specac).

Elemental CHN analysis was carried out using a Carlo Erba CHNS3 FA 1108 Elemental Analyzer. Analysis of boron content was conducted using ICP MS on an iCAP 6300 Duo inductively coupled plasma–atomic emission spectrometer at the IREA Shared Analytical Facilities Center of the National Research Center "Kurchatov Institute".

X-ray powder diffraction (XRD) patterns were recorded with a Bruker D8 Advance diffractometer operating in a Bragg-Brentano geometry using Cu Kα radiation in the 2θ range 3–120° at a 2θ step of 0.02° and a counting time of 0.3 s per step.

The microstructure (scanning electron microscopy, SEM) of the samples was analyzed on a Carl Zeiss NVision 40 high resolution scanning electron microscope equipped with an Oxford

Instruments X-MAX (80 mm$^2$) energy dispersive detector. SEM images were recorded using an Everhart-Thornley detector (SE2) at 1 kV accelerating voltage. Before the measurements, the samples were ground and analyzed without application of any conductive layer on their surface.

The skeletal density ($\rho_{sk}$) of aerogels was measured with a helium pycnometer, Thermo Fisher Scientific Pycnomatic ATC.

The specific surface area ($S_{BET}$) of aerogels was measured using a low-temperature nitrogen adsorption method on a QuantaChrome Nova 4200B analyzer. Prior to analysis, the samples were degassed at 90°C *in vacuo* for 17 h. $S_{BET}$ was calculated using the Brunauer–Emmett–Teller model (BET) within the partial pressure range of 0.07–0.25 (7 experimental points). The pore size distribution was carried out using desorption branches of full nitrogen desorption isotherms according to the Barrett-Joyner-Halenda (BJH) model.

Thermal analysis of aerogels, as well as the identification of gaseous products evolved during thermal decomposition of the samples, was performed using a NETZSCH STA 409 PC Luxx synchronous thermal analyzer combined with a NETZSCH QMS 403 C Aëolos quadrupole mass spectrometer. The analysis was carried out in air at a heating rate of 10 °C/min to 800 °C.

### *2.6 Neutron capture property*

The neutron capture properties of the aerogel samples were studied using two different setups, "Yellow submarine" (BNC reactor, Budapest, Hungary) and KWS-3 (FRM-II reactor, Garching, Germany).

A "Yellow submarine" small-angle diffractometer operates at an approximately point geometry. The use of the neutron wavelength $\lambda = 0.46$ nm ($\Delta\lambda/\lambda = 0.18$) and the sample-to-detector distance $SD = 1.2$ m allowed for the measurements in the momentum transfer range of $q < 3.6$ nm$^{-1}$ (here, $q = 4\pi\lambda^{-1}\sin(\theta/2)$ and $\theta$ is the scattering angle). The neutrons were detected by a two-dimensional position-sensitive $BF_3$ gas detector (64 × 64 cells, 1 cm × 1 cm each).

A KWS-3 setup is a high-resolution small-angle diffractometer, the use of the neutron wavelength $\lambda = 1.28$ nm ($\Delta\lambda/\lambda = 0.2$) and the $SD = 1$ m allowed for the measurements in the momentum transfer range of $q < 0.15$ nm$^{-1}$. The neutrons were detected by a two-dimensional position-sensitive scintillation $^6$Li detector (active spot ∅ = 8.7 cm with a spatial resolution of 0.36×0.39 mm).

In the experiments performed using both setups, the measurements were conducted without a beamstop. The aerogel powders were placed into a quartz cuvette with an optical path of 2 mm, and the neutron intensity was measured at the entire area of the detector. As a reference, an empty cuvette was used (see Fig. S1).

The attenuation of neutron beam by the aerogel sample was estimated using the equation:

$$1 - T_a = 1 - \frac{I(q)}{I_0(q)} = 1 - e^{-\sigma_a \cdot L}, \quad (1)$$

where $I(q)$ и $I_0(q)$ are the distribution function of the neutron beam intensity after transmission through the aerogel sample and the empty cell, respectively; $T_a$ is the transmission coefficient due to absorption and incoherent scattering. The experimental estimates are presented in Table 1. The theoretical neutron attenuation values were estimated using NIST Neutron Activation and

Scattering Calculator[51] basing on the experimentally determined chemical composition of the aerogels, their density and neutron wavelength.

**Table 1.** Theoretical (calc) and experimental (exp) values for the neutron beam attenuation values for **$SiO_2$–B** aerogel sample.

| Neutron beam setup | Neutron wavelength λ, Å | $(1 - T_a)_{exp.}$, % | $(1 - T_a)_{calc.}$, % |
|---|---|---|---|
| "Yellow submarine" | 4.6 | 8.5 ± 0.3 | 7.9 |
| KWS-3 | 12.8 | 20.3 ± 0.3 | 19.8 |

### *2.7 Biocompatibility study*

For the evaluation of biocompatibility of the samples, MTT-test was applied, which was performed using two cell cultures, human glioblastoma (line U251 MG) and human mesenchymal stem cells (DPSc). DPSc were isolated and collected according to recently reported procedure [52]. All procedures were carried out in accordance with the approved clinical rules for biomaterial sampling. Glioblastoma cells (line U251 MG) were obtained from the cryobank of the Institute of Biophysics of the Russian Academy of Sciences (Puschino, Russia).

For biocompatibility studies, the cells were seeded in 96-well plates at a density of 20 000 $cm^{-2}$. After 12 h of cultivation, the DMEM/F-12 culture medium was completely replaced with an identical medium containing 0.01–0.5 mg/ml powders of **$SiO_2$** or **$SiO_2$–B** aerogels. The activity of mitochondrial and cytoplasmatic dehydrogenases of the living cells was estimated using a standard MTT-test. The cell viability was analyzed after 24 and 72 h of cultivation with **$SiO_2$** or **$SiO_2$–B** aerogels.

## 3. Results and discussion

### 3.1 Synthesis of N-borylated alkoxy silane

For the synthesis of *closo*-decaborate anion derivatives, we used an approach based on nucleophilic addition of amine to a multiple bond of niltrilium compounds. First, acetonitrilium derivative is formed through electrophile-induced nucleophilic substitution.[39] Then activated nitrilium group reacts with primary amine *via* nucleophilic addition mechanism.[53] This approach was successfully applied earlier for the synthesis of *closo*-decaborates with various substituents, including biologically active compounds.[54] The reaction is conducted under mild conditions, providing high yield of the reaction product, which can easily be extracted from the reaction mixture.

For the synthesis of new alkoxysilylated *closo*-decaborate cluster, **APTES-B**, we used 3-aminopropyl triethoxysilane (APTES) as a nucleophile. The synthesis product contains hydrolysable ethoxysilanol groups which can be chemically immobilized onto silica aerogel matrix (Fig. 1).

The synthesis of **APTES-B** was conducted in dichloromethane under argon at ambient temperature. The reaction process was controlled using $^{11}B$ NMR spectroscopy. Complete conversion of initial nitrilium derivative (**CNB**) was observed in 1.5 h. In **APTES-B** spectrum, a singlet signal at –14.5 ppm (integral intensity $I = 1$) from substituted boron atom is observed, non-substituted boron atoms provide dublet signals. The signals from non-symmetric apical boron atoms are observed at 3.5 ppm ($I = 1$) and –3.7 ppm ($I = 1$), the signals from non-substituted equatorial boron atoms are observed at –23.3 ppm ($I = 4$) and –26.3 ppm ($I = 3$) (Fig. S2).

The structure of substituent in **APTES-B** was analysed using $^{1}H$ and $^{13}C$ NMR spectroscopy. $^{1}H$ NMR spectrum of **APTES-B** contains signals attributed to tetrabutyl ammonium cation and signals from hydrogen atoms of *exo*-polyhedric substituent. Methyl protons provide singlet signal at 1.98 ppm, aliphatic protons provide three signals at 2.62 ppm, 1.79 ppm and 0.74 ppm. Ethoxide groups give two signals at 3.83 ppm and 1.22 ppm. Amidinium fragment gives two broadened singlets at 8.41 ppm (N*H*-Alk) and 5.73 ppm (N*H*=C–). $^{13}C$ NMR spectrum of **APTES-B** (Fig. S2) is analogous to the spectra of a family of N-borylated amidines [55]. Amidine moiety provides signals at 165.1 ppm (N=**C**$CH_3$) and 24.1 ppm (N=C**C**$H_3$). Ethoxide fragments at silicon atom give signals at 59.1 ppm (O**C**$H_2CH_3$) and 18.9 ppm ($OCH_2$**C**$H_3$), alkyl moiety at silicon atom provides three signals at 46.7 ppm (**C**$H_2CH_2CH_2Si$), 20.1 ppm ($CH_2$**C**$H_2CH_2Si$) and 8.2 ppm ($CH_2CH_2$**C**$H_2Si$).

In mass spectra of **APTES-B**, anionic component is present at *m*/*z* 379.50, as well as a series of peaks related to the de-ethoxylated products, *m*/*z* 336.91 and *m*/*z* 325.41. In IR spectra of **APTES-B**, the most characteristic bands are related to stretching B–H vibrations of boron cluster at 2477 $cm^{-1}$, as well as absorption bands of N–H stretching vibrations from amidinium moiety at 3338, 3313 and 3267 $cm^{-1}$, and C=N stretching vibrations at 1648 $cm^{-1}$ (Fig. 2).

Previously, silylated *closo*-decaborates $[1\text{-}B_{10}H_9NH_2(CH_2)_2NHCONH(CH_2)_3Si(OEt)_3]^-$ and $[2\text{-}B_{10}H_9CONH(CH_2)_3Si(OEt)_3]^{2-}$ were successfully synthesised by Abi-Ghaida *et al.*[43,44] Their attempt to synthesise amidinium *closo*-decaborate derivative $[2\text{-}B_{10}H_9NC(CH_2)_3Si(OEt)_3]^-$ using 3-cyanopropyl triethoxysilane resulted in an inseparable mixture of three different borylated derivatives.[43] Generally, borylated amidines are much less prone to hydrolysis than ester-type derivatives,[56,57] that guarantees a strong chemical immobilisation of *closo*-decaborate cage on the surface of silica under acidic or basic environment. Our synthetic protocol allowed for the selective synthesis of a substituted amidinium derivative of a *closo*-decaborate cluster.

### 3.2 Synthesis of lyogels

Sol-gel transition during the synthesis of unmodified **$SiO_2$** gel was initiated with aqueous ammonia. In the case of **$SiO_2$–B** synthesis, the addition of **APTES-B** itself to a $SiO_2$ sol led to an increase in the pH of the system and caused sol-gel transition due to the presence of the –NH– moieties in **APTES-B**.

After ageing, the gels were washed with isopropanol 5 times to replace the solvent with pure isopropanol and to remove weakly bound **APTES-B** molecules. The washing solutions were collected and further analyzed by means of $^{11}B$ NMR and IR spectroscopy. Fig. S3 presents $^{11}B$ NMR spectrum for the **CNB** compound and $^{11}B$ NMR spectra of the first three washing solutions. The spectra indicate that they do not contain any notable amounts of the **APTES-B**, the leeching from the material did not exceed 0.5 mol.% of the total boron content. IR absorbance spectra corroborate this result by the absence of intense bands inherent in **APTES-B**, which confirm the immobilization of **APTES-B** in $SiO_2$ lyogel matrix.

### 3.3 Borylated silica aerogels: synthesis, composition and microstructure

Monolithic aerogels were obtained by supercritical drying of lyogel samples in $CO_2$ (Fig. S4). Synthesis of the **$SiO_2$–B** aerogel resulted in non-transparent monoliths.

Fig. 2 shows IR spectra of **APTES-B** precursor and **$SiO_2$** and **$SiO_2$–B** aerogels. In IR spectrum of **$SiO_2$–B** aerogel, several absorbance bands are present due to B–H stretching vibrations at 2480–2470 cm$^{-1}$, C–H stretching vibrations at 2800–300 cm$^{-1}$ and C=N stretching vibrations at 1650 cm$^{-1}$.[58] In the IR spectrum of **$SiO_2$–B** aerogel sample, a shoulder at 880 cm$^{-1}$ can be attributed to Si–C stretching vibrations (see *e.g.* recently reported data[59]).

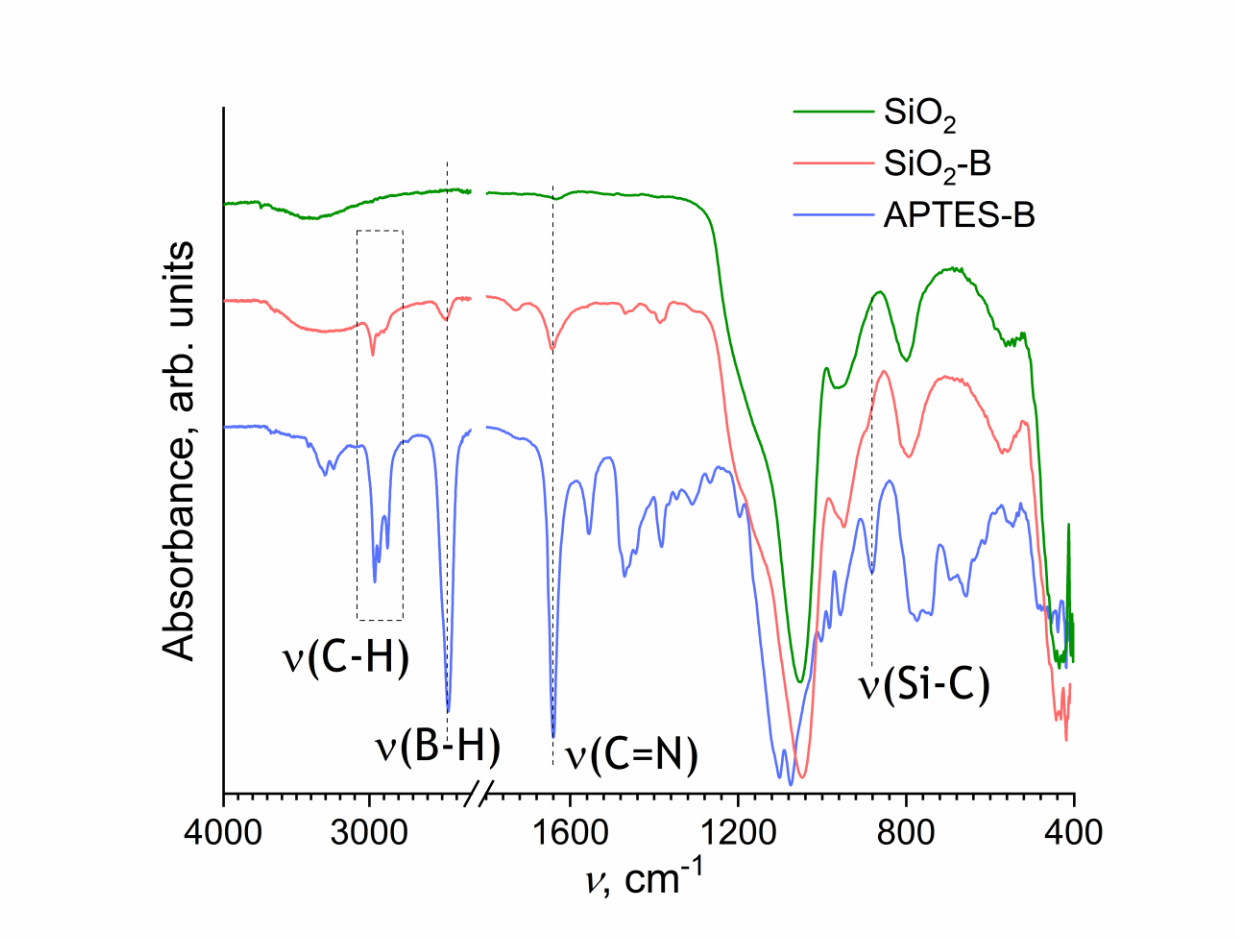


**Figure 2.** IR spectra of **APTES-B**, boron-containing aerogel **$SiO_2$–B** and unmodified **$SiO_2$** aerogel.

Elemental analysis has shown that the content of boron clusters in **$SiO_2$–B** aerogel is 1.2 mol.%, which is almost equal to theoretical value of 1.5 mol.%. These data also corroborate the successful immobilization of *closo*-decaborate cluster in the silica aerogel matrix.

Solid state $^{11}$B MAS NMR indicate the presence of **APTES-B** moieties in **$SiO_2$–B** aerogel (Fig. 3). **$SiO_2$–B** $^{11}$B MAS NMR spectrum is almost identical to **APTES-B** spectrum, indicating the inheritance of the structure of substituted boron cluster in aerogel matrix. **APTES-B** $^{11}$B MAS

NMR spectrum comprises four broadened signals, a complex signal in strong field at –27.8 ppm corresponds to non-substituted boron atoms located in equatorial belt of *closo*-borate cluster, a signal at –17.4 ppm corresponds to substituted boron atom. The signals from apical boron clusters are registered in weak field at –1.5 ppm and –4.9 ppm. The broadening of the lines in solid state $^{11}B$ MAS NMR spectrum of $SiO_2$-B aerogel is most probably due to the low total boron content in a measurement cell which is due to the low apparent density of the material (see Table 2).

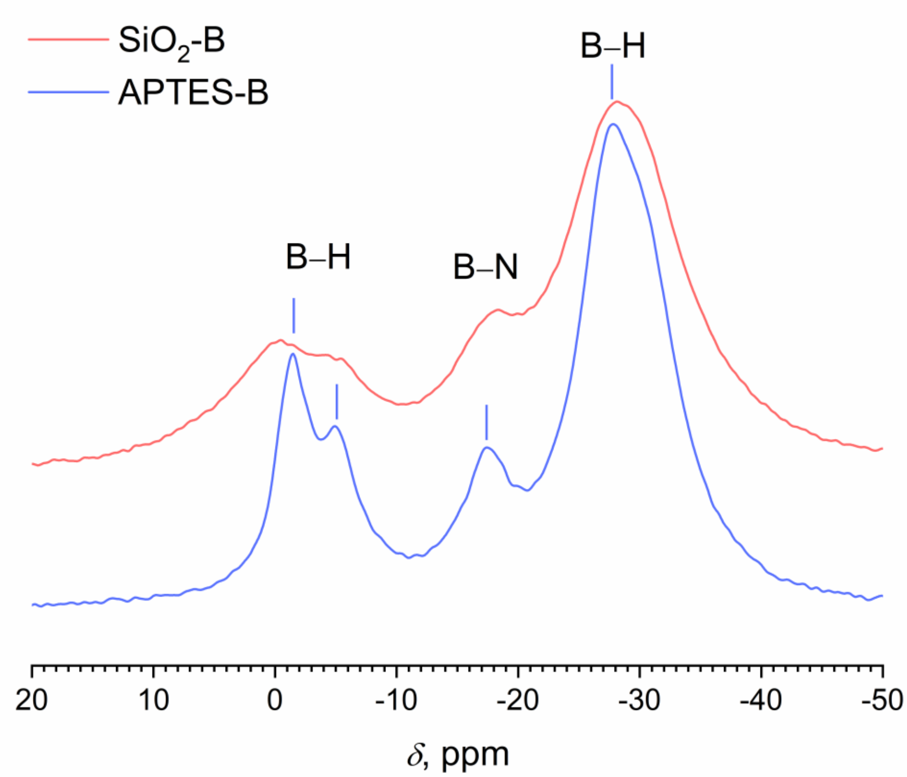


**Figure 3.** Solid state $^{11}B$ MAS NMR spectra of **APTES-B** and boron-modified **$SiO_2$–B** aerogel.

Thus, IR and NMR spectroscopy data support the successful immobilization of a *closo*-borate cluster derivative **APTES-B** in the $SiO_2$ aerogel matrix.

Table 2 summarises textural characteristics of aerogel modified with a *closo*-decaborate cluster and of unmodified silica aerogel synthesized under similar conditions. These data show that modification of aerogel with *closo*-decaborate derivative results in only minor changes in apparent density and porosity of the resultant material. Boron-modified aerogel exhibits very high specific surface, 740 $m^2$/g, being only ~15 % lower than that of unmodified silica. The silica aerogel bearing *closo*-decaborate clusters possessed very low apparent density values (~80 mg/$cm^3$) that make this material beneficial for the creation of shielding covers for the patients with heavily impaired health. Note that the apparent density for the ultralight silica xerogel materials is at least twice as high with the most common values being ~200 mg/$cm^3$.[60]

**Table 2.** Textural characteristics of $\mathbf{SiO_2}$ and $\mathbf{SiO_2}$**–B** aerogels.

| | $\mathbf{SiO_2}$ | $\mathbf{SiO_2}$**–B** |
|---|---|---|
| Nominal molar ratio, B:Si | – | 0.15 |
| Experimental molar ratio B:Si | – | 0.12 |
| Gelling duration, $\tau_{gel}$, s | 1800±100 | 15±3 |
| Apparent density, $\rho_{geom}$, g·cm$^{-3}$ | 0.07±0.01 | 0.08±0.01 |
| Porosity, $P$, % | 96±3 | 96±3 |
| Specific surface, $S_{sp}$, m$^2$·g$^{-1}$ | 860±60 | 740±50 |
| Specific pore volume, $V_{por}$, cm$^3$·g$^{-1}$ | 3.89 | 5.56 |
| Average pore diameter, $D_{por}$, nm | 13 | 17 |
| Particle size, $D_{TEM}$, nm | 3±1 | 11±3 |

Full nitrogen adsorption-desorption isotherms and pore size distributions for $\mathbf{SiO_2}$ and $\mathbf{SiO_2}$**–B** aerogels are presented in Fig. S5. Both of the isotherms are of IUPAC IV(a) type typical to mesoporous adsorbents.[61] The hysteresis loop for $\mathbf{SiO_2}$ is close to H1 type indicating the presence of a narrow range of uniform mesopores.[61] A pronounced increase in adsorption values for $\mathbf{SiO_2}$**–B** aerogel at high nitrogen partial pressures ($P/P_0 \sim 1$) indicates that relatively large pores (> 50 nm) and even macropores are present in its structure. Due to the presence of macropores, the exact classification of the hysteresis loop type for the $\mathbf{SiO_2}$**-B** aerogel is more complex, it can be related to either H1 or H2(b) type. The latter is characteristic of materials with partially blocked pores and wide pore neck widths distribution.[61] The high content of large pores in $\mathbf{SiO_2}$**–B** sample follows from the pore size distribution curve calculated using BJH model (Fig. S5) and from the higher value of specific pore volume relative to $\mathbf{SiO_2}$ aerogel sample (see Table 2). Thus, immobilization of *closo*-decaborate cluster in $SiO_2$ matrix results in certain changes in aerogel structure, which is also evidenced from SEM data (see Fig. 4). SEM images confirm the presence of larger pores and macropores in $\mathbf{SiO_2}$**–B** aerogel.

Transmission electron microscopy (Table 2, Fig. 4a) shows that co-gelation of TEOS and **APTES-B** results in formation of gels with particles 3–4 times larger compared to control TEOS-derived gels (Table 2). According to low temperature nitrogen adsorption and SEM data (Fig. 4b), the structure of $\mathbf{SiO_2}$**–B** aerogel contains both small and large pores and particle aggregates. Such inhomogeneous porous structure is responsible for optical opacity of $\mathbf{SiO_2}$**–B** aerogel monolith (Fig. S4). The observed differences in the microstructure of $\mathbf{SiO_2}$ and $\mathbf{SiO_2}$**–B** aerogels are related to the different rates of gelation process (gelling duration $\tau$, see Table 2). Co-gelation of TEOS and **APTES-B** occurs at a much more rapid rate than that of TEOS alone, which is a quite unusual effect bearing in mind the presumably low basicity of the amidinium derivative of *closo*-decaborate. Most probably, such a difference in gelation rates is due to the hydrogen bonding of *closo*-decaborate moiety with water or alcohol molecules in its microenvironment.

Higher gel formation rates result in more ramified colloid structures possessing wider pore size distribution (see Fig. S5). This contributes to the higher average pore diameter and specific pore volume in $\mathbf{SiO_2}$**–B** aerogel compared to the unmodified $\mathbf{SiO_2}$ material. Increased basicity of the medium also favours the formation of large aggregates as evidenced from TEM data (Table 2, Fig. 4a).

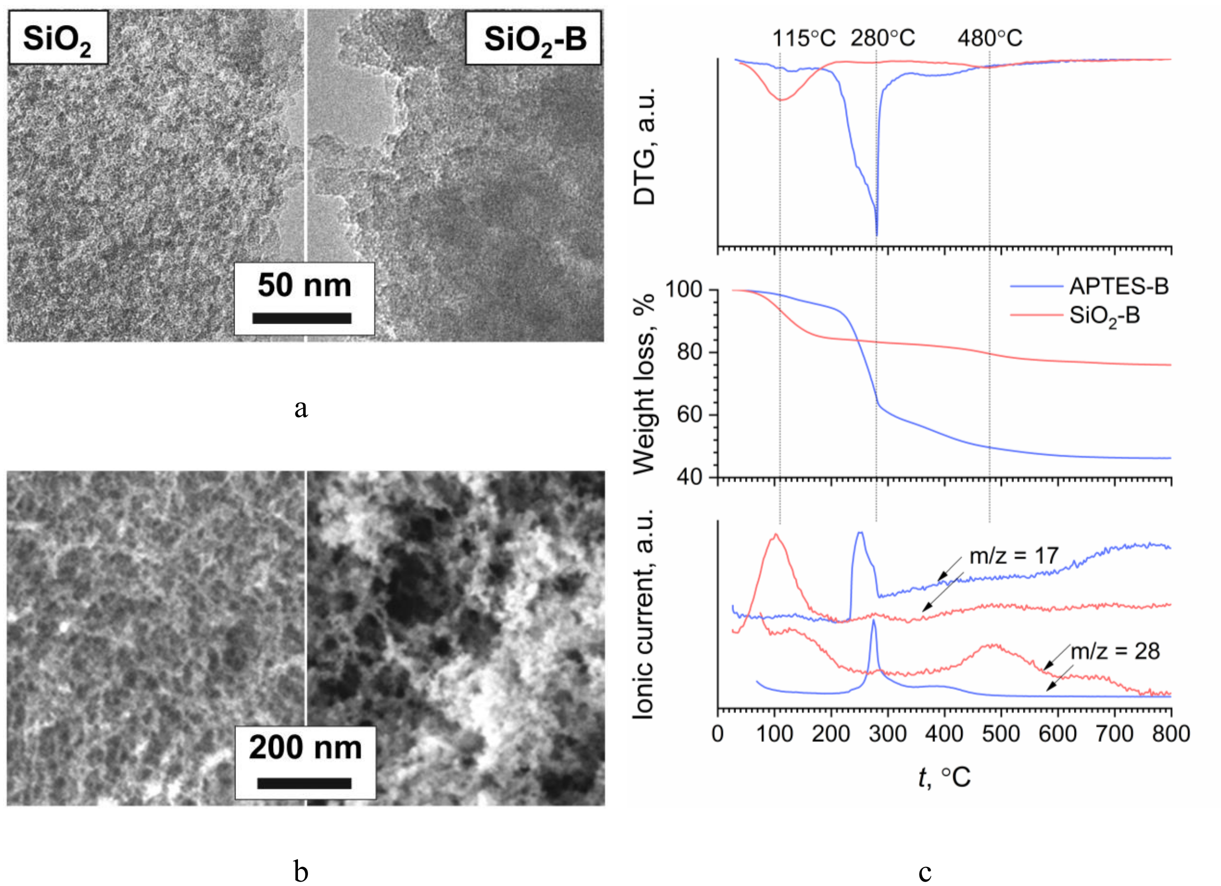


**Figure 4.** (a) TEM and (b) SEM images of $\mathbf{SiO_2}$ and $\mathbf{SiO_2}$**–B** aerogels; (c) the results of thermal analysis (in argon atmosphere) coupled with mass-spectrometry of the evolved gases for **APTES–B** and $\mathbf{SiO_2}$**–B** aerogel.

Fig. 4c shows the results of the thermal analysis of **APTES-B** and $\mathbf{SiO_2}$**–B** aerogels coupled with mass-spectrometry of the gaseous products evolved upon heating in argon. Thermal decomposition of **APTES-B** begins at 210 °C, while the decomposition of boron cluster in $\mathbf{SiO_2}$**–B** begins at higher temperature (350–400 °C) indicating increased thermal stability of a *closo*-decaborate moiety in aerogel matrix. Increased thermal stability of coordination compounds immobilized in porous matrices seems to be a common feature of hybrid materials, which was discussed elsewhere.[62] The effect is probably caused by a thermal insulation property of the aerogel matrix protecting *closo*-decaborate moieties from thermal attack.[62]

### 3.4 Neutron capture properties of $SiO_2$–B aerogels

*closo*-Decaborate clusters contain both $^{10}$B isotope (approximately 20% natural abundance)[4] possessing high thermal neutron cross-section value,[3] and high amount of hydrogen (~8.5 wt.%) which acts as neutron moderator. Silica matrix also contains high amount of chemically bound hydrogen (as hydroxyls, water molecules and organic moieties). Thus the material comprising both boron clusters and silica matrix can act as both effective neutron moderator and absorber. Table 3 summarises the neutron capture property of **$SiO_2$-B** aerogel material at neutron flux density of $\Phi = 10^7$ $cm^{-2}s^{-1}$ and various neutron wavelengths, which are the most commonly used at neutron scattering facilities. The parameter *L* is the width of aerogel layer providing the reducing of neutron beam intensity by a factor of *e*. In Table 3, the neutron absorption cross-section and penetration depth values for 4.6 Å and 12.8 Å were estimated using experimentally measured beam attenuation (see Table 1) for 2 mm thick aerogel samples; the values for 1 Å were calculated using NIST Neutron Activation and Scattering Calculator[51] considering the chemical composition of aerogels and taking in mind the good agreement of experimental and calculated beam attenuation values (Table 1).

**Table 3.** The neutron capture property of bare **$SiO_2$** and **$SiO_2$-B** aerogel materials.

| **Neutron wavelength, $\lambda$, Å** | **Neutron absorption cross section, $\sigma_a$, $cm^{-1}$** | | **Absorption penetration depth, *L*, cm** | |
|---|---|---|---|---|
| | **$SiO_2$** | **$SiO_2$-B** | **$SiO_2$** | **$SiO_2$-B** |
| **1** | 0.01* | 2.2* | 3800* | 12* |
| **4.6** | 0.03 | 9.7 | 825 | 3 |
| **12.8** | 0.09 | 26.9 | 295 | 1 |

*Calculated values

Comparison of the neutron absorption property of similar materials reported elsewhere[63] with the characteristics of **$SiO_2$-B** aerogel shows excellent performance of the latter and its high potential for practical applications. For example, thermal neutron macroscopic cross section of natural rubber / boric acid composites reached only 0.29 $cm^{-1}$;[64] polyvinyl alcohol / high density polyethylene / $B_4C$ composites – 1.72 $cm^{-1}$;[65] similar values, not exceeding 2.5 $cm^{-1}$, were reached for other boron-containing polymer-based composites.[66–69] The highest reported value for the relatively light polymer-based neutron shielding materials reached ~15 $cm^{-1}$ for thermoplastic natural rubber / $B_4C$ composite with 30 wt.% $B_4C$ loading (the neutron wavelength value was not provided). We believe that the increase in boron clusters content in **$SiO_2$-B** aerogels would result in even better neutron absorption characteristics of the material.

### 3.5 Cell viability test

For the use in personnel safety wears, aerogel material needs to possess low toxicity. This property is of special importance for the shielding of patients with heavily impaired health. In view of this promising use, a comparative survey of the viability of normal (dental pump stem cells) and malignant (U251 MG glioblastoma line) cells in the presence of **$SiO_2$-B** aerogel was performed (Fig. 5).

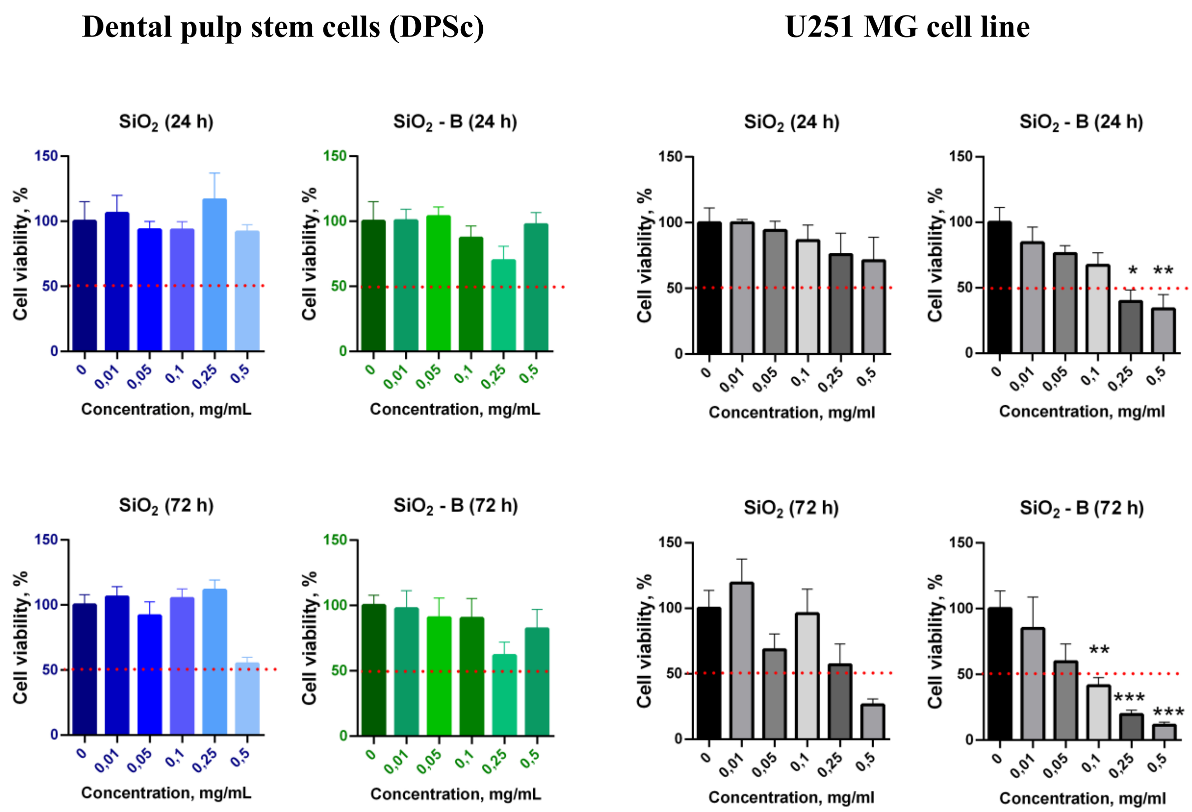


**Figure 5.** Viability of dental pump stem cells (DPSc) and U251 MG cells after incubation with pure $SiO_2$ and modified $SiO_2$–B aerogels (MTT assay after 24 and 72 h). Data are presented as mean±SD (yEr±), $n = 3$. * – p 0.05, ** – p 0.01, *** – p 0.0001.

The data show the high toxicity of boron-modified aerogel material with respect to malignant cells. Upon 24 h of incubation a reliable decrease in U251 MG cell viability is observed at aerogel concentration of 0.5 mg/ml. After 72 h, a decrease in cell viability (more than 50%) is observed at a far less **$SiO_2$-B** concentrations (0.05 mg/ml). At the same time, the toxicity of **$SiO_2$-B** sample to stem cells was substantially lower – no toxic effect was observed upon 24 h of incubation in concentrations up to 0.5 mg/ml. Only upon 72 h of stem cells incubation with aerogel material taken in high concentration (0.25–0.5 mg/ml) a certain decrease in DPSc viability was observed. The reasons for such a different response of normal and malignant cells need further clarification, they can be connected to both differences in their metabolism and endocytosis of aerogel particles.

Thus, the borylated aerogel material possessed low cytotoxicity with respect to normal cells. This result ascertains the safety in the use of borylated aerogels for the use in the neutron shields for the oncology patients and health personnel involved in boron neutron caption therapy procedures.

## 4. Conclusions

Interaction of $[2\text{-}B_{10}H_9(NCCH_3)]^-$ with $NH_2(CH_2)_3Si(OCH_2CH_3)_3$ yielded a new silylated *closo*-decaborate cluster, $[2\text{-}B_{10}H_9\{Z\text{-}NH{=}C(CH_3)NH(CH_2)_3Si(OCH_2CH_3)_3\}]^-$. The silylated *closo*-decaborate was successfully immobilized onto $SiO_2$ aerogel matrix resulting in an aerogel nanomaterial containing 1.2 mol.% *closo*-decaborate moieties. The borylated silica aerogel nanomaterial possessed high specific surface area (740 $m^2/g$) and open porosity (95 %) as well as low apparent density (80 $mg/cm^3$). The material showed low toxicity with respect to normal cells, while was cytotoxic to malignant glyoblasoma cells. The *closo*-decaborate modified aerogel showed excellent neutron capture properties, neutron absorption cross-section reached 26 $cm^{-1}$ for the neutron beam with $\lambda = 12$ Å. The combination of the properties of *closo*-decaborate modified silica aerogels make them good candidate material for shielding of patients and healthcare personnel during boron neutron capture therapy procedures.

The strategy for the synthesis of silica sol-gel materials where boron clusters are chemically immobilised in $SiO_2$ matrix directly at the co-condensation stage of silicon compounds is applicable to the synthesis of wide variety of silica-based materials, including aerogels, xerogels, and ambigels.

**Supporting Information.** Scheme of the neutron capturing property experiment, $^{11}$B NMR, $^{13}$C NMR spectra, full nitrogen adsorption-desorption isotherms and the appearance of the samples.

AUTHOR INFORMATION

**Corresponding Author**

* van@igic.ras.ru

**Author Contributions**

The manuscript was written through contributions of all authors. All authors have given approval to the final version of the manuscript.

**Funding Sources**

This work was supported by the Russian Science Foundation (19-73-20125).

ACKNOWLEDGMENT

The research was performed using the equipment of the Joint Research Center for Physical Methods of Research in Kurnakov Institute of General and Inorganic Chemistry of the Russian Academy of Sciences. The authors are very grateful to Dr. V. Pipich and the Heinz Maier-Leibnitz Zentrum for the kind assistance in conducting neutron measurements. TOC graphic and Fig. S1 were created with BioRender.com.

REFERENCES

(1) *Micro and Nanostructured Composite Materials for Neutron Shielding Applications*; Abdulrahman, S. T., Thomas, S., Ahmad, Z., Eds.; Elsevier, 2020. https://doi.org/10.1016/C2019-0-00001-5.

(2) Nedunchezhian, K. Boron Neutron Capture Therapy - A Literature Review. *J. Clin. DIAGNOSTIC Res.* **2016**. https://doi.org/10.7860/JCDR/2016/19890.9024.

(3) Lee, G. H.; Chang, Y.; Kim, T.-J. Thermal Neutron Capture Therapy (NCT). In *Ultrasmall Lanthanide Oxide Nanoparticles for Biomedical Imaging and Therapy*; Elsevier, 2014; pp 97–102. https://doi.org/10.1533/9780081000694.97.

(4) Wieser, M. E.; Coplen, T. B. Atomic Weights of the Elements 2009 (IUPAC Technical Report). *Pure Appl. Chem.* **2010**, *83* (2), 359–396. https://doi.org/10.1351/PAC-REP-10-09-14.

(5) Fu, X.; Ji, Z.; Lin, W.; Yu, Y.; Wu, T. The Advancement of Neutron Shielding Materials for the Storage of Spent Nuclear Fuel. *Sci. Technol. Nucl. Install.* **2021**, *2021*, 1–13. https://doi.org/10.1155/2021/5541047.

(6) Mortazavi, S. M. J.; Kardan, M.; Sina, S.; Baharvand, H.; Sharafi, N. Design and Fabrication of High Density Borated Polyethylene Nanocomposites as a Neutron Shield. *Internatuinal J. Radiat. Res.* **2016**, *14* (4), 379–383. https://doi.org/10.18869/acadpub.ijrr.14.4.379.

(7) Roy, S. C.; Sandison, G. A. Shielding for Neutron Scattered Dose to the Fetus in Patients Treated with 18 MV X-Ray Beams. *Med. Phys.* **2000**, *27* (8), 1800–1803. https://doi.org/10.1118/1.1287438.

(8) Pierre, A. C.; Rigacci, A. SiO2 Aerogels. In *Aerogels Handbook*; Springer New York: New York, NY, 2011; pp 21–45. https://doi.org/10.1007/978-1-4419-7589-8_2.

(9) Chen, H.-B.; Ao, Y.-Y.; Liu, D.; Song, H.-T.; Shen, P. Novel Neutron Shielding Alginate Based Aerogel with Extremely Low Flammability. *Ind. Eng. Chem. Res.* **2017**, *56* (30), 8563–8567. https://doi.org/10.1021/acs.iecr.7b01999.

(10) Harrison, C.; Weaver, S.; Bertelsen, C.; Burgett, E.; Hertel, N.; Grulke, E. Polyethylene/Boron Nitride Composites for Space Radiation Shielding. *J. Appl. Polym. Sci.* **2008**, *109* (4), 2529–2538. https://doi.org/10.1002/app.27949.

(11) Li, X.; Wu, J.; Tang, C.; He, Z.; Yuan, P.; Sun, Y.; Lau, W.; Zhang, K.; Mei, J.; Huang, Y. High Temperature Resistant Polyimide/Boron Carbide Composites for Neutron Radiation Shielding. *Compos. Part B Eng.* **2019**, *159*, 355–361. https://doi.org/10.1016/j.compositesb.2018.10.003.

(12) Nelson, K. A.; Bellinger, S. L.; Montag, B. W.; Neihart, J. L.; Riedel, T. A.; Schmidt, A. J.; McGregor, D. S. Investigation of Aerogel, Saturated Foam, and Foil for Thermal Neutron Detection. In *2011 IEEE Nuclear Science Symposium Conference Record*; IEEE, 2011; pp 1026–1029. https://doi.org/10.1109/NSSMIC.2011.6154313.

(13) Yorov, K. E.; Baranchikov, A. E.; Kiskin, M. A.; Sidorov, A. A.; Ivanov, V. K. Functionalization of Aerogels with Coordination Compounds. *Russ. J. Coord. Chem.* **2022**, *48* (2), 89–117. https://doi.org/10.1134/S1070328422020014.

(14) Martínez, S.; Moreno-Mañas, M.; Vallribera, A.; Schubert, U.; Roig, A.; Molins, E. Highly Dispersed Nickel and Palladium Nanoparticle Silica Aerogels: Sol-Gel Processing of Tethered

Metal Complexes and Application as Catalysts in the Mizoroki-Heck Reaction. *New J. Chem.* **2006**, *30* (7), 1093–1097. https://doi.org/10.1039/b604544h.

(15) Yorov, K. E.; Yapryntsev, A. D.; Baranchikov, A. E.; Khamova, T. V.; Straumal, E. A.; Lermontov, S. A.; Ivanov, V. K. Luminescent Alumina-Based Aerogels Modified with Tris(8-Hydroxyquinolinato)Aluminum. *J. Sol-Gel Sci. Technol.* **2018**, *86* (2), 400–409. https://doi.org/10.1007/s10971-018-4647-5.

(16) Murphy, E. F.; Schmid, L.; Bürgi, T.; Maciejewski, M.; Baiker, A.; Günther, D.; Schneider, M. Nondestructive Sol-Gel Immobilization of Metal(Salen) Catalysts in Silica Aerogels and Xerogels. *Chem. Mater.* **2001**, *13* (4), 1296–1304. https://doi.org/10.1021/cm001187w.

(17) Seçkin, T.; Çetinkaya, B.; Özdemir, I. Sol-Gel Synthesis of Ru(II) Complex of 3-4,5-Dihydroimidazol-1-Yl-Propyltriethoxysilane Aerogels and Xerogels. *Polym. Bull.* **2000**, *44* (1), 47–53. https://doi.org/10.1007/s002890050572.

(18) Poater, J.; Solà, M.; Viñas, C.; Teixidor, F. Hückel's Rule of Aromaticity Categorizes Aromatic Closo Boron Hydride Clusters. *Chem. – A Eur. J.* **2016**, *22* (22), 7437–7443. https://doi.org/10.1002/chem.201600510.

(19) Núñez, R.; Tarrés, M.; Ferrer-Ugalde, A.; de Biani, F. F.; Teixidor, F. Electrochemistry and Photoluminescence of Icosahedral Carboranes, Boranes, Metallacarboranes, and Their Derivatives. *Chem. Rev.* **2016**, *116* (23), 14307–14378. https://doi.org/10.1021/acs.chemrev.6b00198.

(20) Fink, K.; Uchman, M. Boron Cluster Compounds as New Chemical Leads for Antimicrobial Therapy. *Coord. Chem. Rev.* **2021**, *431*, 213684. https://doi.org/10.1016/j.ccr.2020.213684.

(21) Sivaev, I. B.; Prikaznov, A. V.; Naoufal, D. Fifty Years of the Closo-Decaborate Anion Chemistry. *Collect. Czechoslov. Chem. Commun.* **2010**, *75* (11), 1149–1199. https://doi.org/10.1135/cccc2010054.

(22) Ali, F.; S Hosmane, N.; Zhu, Y. Boron Chemistry for Medical Applications. *Molecules* **2020**, *25* (4), 828. https://doi.org/10.3390/molecules25040828.

(23) Li, H.; Zhang, Y.; Liu, L.; Jiao, N.; Meng, X.; Zhang, S. Amino Functionalized [B 12 H 12 ] 2− Salts as Hypergolic Fuels. *New J. Chem.* **2018**, *42* (5), 3568–3573. https://doi.org/10.1039/C7NJ04225F.

(24) Brighi, M.; Murgia, F.; Łodziana, Z.; Schouwink, P.; Wołczyk, A.; Cerny, R. A Mixed Anion Hydroborate/Carba-Hydroborate as a Room Temperature Na-Ion Solid Electrolyte. *J. Power Sources* **2018**, *404*, 7–12. https://doi.org/10.1016/j.jpowsour.2018.09.085.

(25) Huang, Z.; Wang, S.; Dewhurst, R. D.; Ignat'ev, N. V.; Finze, M.; Braunschweig, H. Boron: Its Role in Energy-Related Processes and Applications. *Angew. Chemie Int. Ed.* **2020**, *59* (23), 8800–8816. https://doi.org/10.1002/anie.201911108.

(26) Jankowiak, A.; Baliński, A.; Harvey, J. E.; Mason, K.; Januszko, A.; Kaszyński, P.; Young, V. G.; Persoons, A. [Closo-B 10 H 10 ] 2− as a Structural Element for Quadrupolar Liquid

Crystals: A New Class of Liquid Crystalline NLO Chromophores. *J. Mater. Chem. C* **2013**, *1* (6), 1144–1159. https://doi.org/10.1039/C2TC00547F.

(27) Kapuściński, S.; Abdulmojeed, M. B.; Schafer, T. E.; Pietrzak, A.; Hietsoi, O.; Friedli, A. C.; Kaszyński, P. Photonic Materials Derived from the [ Closo -B 10 H 10 ] 2− Anion: Tuning Photophysical Properties in [ Closo -B 10 H 8 -1-X-10-(4-Y-NC 5 H 5 )] −. *Inorg. Chem. Front.* **2021**, *8* (4), 1066–1082. https://doi.org/10.1039/D0QI01353F.

(28) Zhao, X.; Fu, Y.; Yao, C.; Xu, S.; Shen, Y.; Ding, Q.; Liu, W.; Zhang, H.; Zhou, X. From Boron Organic Polymers to in Situ Ultrafine Nano Pd and Pt: Green Synthesis and Application for High Efficiency Hydrogen Evolution. *ChemCatChem* **2019**, *11* (9), 2362–2369. https://doi.org/10.1002/cctc.201900281.

(29) Wang, Z.; Wang, Z.; Ma, X.; Liu, Y.; Zhang, H. Direct Conversion of Methane into Methanol and Ethanol via Spherical Au@Cs2[Closo-B12H12]and Pd@Cs2[Closo-B12H12] Nanoparticles. *Int. J. Hydrogen Energy* **2021**. https://doi.org/10.1016/j.ijhydene.2021.06.196.

(30) Shakirova, O. G.; Daletskii, V. A.; Lavrenova, L. G.; Trubina, S. V.; Erenburg, S. B.; Zhizhin, K. Y.; Kuzhetsov, N. T. Iron(II) Closo-Borate Complexes with 1,2,4-Triazole Derivatives: Spin Crossover in the Iron(II) Closo-Borate Complexes with Tris(Pyrazol-1-Yl)Methane. *Russ. J. Inorg. Chem.* **2013**, *58* (6), 650–656. https://doi.org/10.1134/S0036023613060211.

(31) Belov, A. S.; Voloshin, Y. Z.; Pavlov, A. A.; Nelyubina, Y. V.; Belova, S. A.; Zubavichus, Y. V.; Avdeeva, V. V.; Efimov, N. N.; Malinina, E. A.; Zhizhin, K. Y.; Kuznetsov, N. T. Solvent-Induced Encapsulation of Cobalt(II) Ion by a Boron-Capped Tris-Pyrazoloximate. *Inorg. Chem.* **2020**, *59* (9), 5845–5853. https://doi.org/10.1021/acs.inorgchem.9b03335.

(32) Sivaev, I. B.; Bregadze, V. I.; Kuznetsov, N. T. Derivatives of the Closo-Dodecaborate Anion and Their Application in Medicine. *Russ. Chem. Bull.* **2002**, *51* (8), 1362–1374. https://doi.org/10.1023/A:1020942418765.

(33) Sivaev, I. B.; Bregadze, V. V. Polyhedral Boranes for Medical Applications: Current Status and Perspectives. *Eur. J. Inorg. Chem.* **2009**, No. 11, 1433–1450. https://doi.org/10.1002/ejic.200900003.

(34) Satapathy, R.; Dash, B. P.; Mahanta, C. S.; Swain, B. R.; Jena, B. B.; Hosmane, N. S. Glycoconjugates of Polyhedral Boron Clusters Dedicated to Professor Russell Grimes on the Occasion of His 80th Birthday. *J. Organomet. Chem.* **2015**, *798*, 13–23. https://doi.org/10.1016/j.jorganchem.2015.06.027.

(35) Losytskyy, M. Y.; Kovalska, V. B.; Varzatskii, O. A.; Kuperman, M. V.; Potocki, S.; Gumienna-Kontecka, E.; Zhdanov, A. P.; Yarmoluk, S. M.; Voloshin, Y. Z.; Zhizhin, K. Y.; Kuznetsov, N. T.; Elskaya, A. V. An Interaction of the Functionalized Closo-Borates with Albumins: The Protein Fluorescence Quenching and Calorimetry Study. *J. Lumin.* **2016**, *169*, 51–60. https://doi.org/10.1016/j.jlumin.2015.08.042.

(36) Viñas i Teixidor, C. The Uniqueness of Boron as a Novel Challenging Element for Drugs in Pharmacology, Medicine and for Smart Biomaterials. *Future Med. Chem.* **2013**, *5* (6), 617–619. https://doi.org/10.4155/fmc.13.41.

(37) Soloway, A. H.; Tjarks, W.; Barnum, B. A.; Rong, F.-G. G.; Barth, R. F.; Codogni, I. M.; Wilson, J. G.; Albert H. Soloway, *; Werner Tjarks; Beverly A. Barnum; Feng-Guang Rong; Rolf F. Barth; Iwona M. Codogni, and; Wilson, J. G.; Soloway, A. H.; Tjarks, W.; Barnum, B. A.; Rong, F.-G. G.; Barth, R. F.; Codogni, I. M.; Wilson, J. G.; Albert H. Soloway, *; Werner Tjarks; Beverly A. Barnum; Feng-Guang Rong; Rolf F. Barth; Iwona M. Codogni, and; Wilson, J. G. The Chemistry of Neutron Capture Therapy. *Chem. Rev.* **1998**, *98* (4), 1515–1562. https://doi.org/10.1021/cr941195u.

(38) Zhizhin, K. Y.; Zhdanov, A. P.; Kuznetsov, N. T. Derivatives of Closo-Decaborate Anion [B10H10]2− with Exo-Polyhedral Substituents. *Russ. J. Inorg. Chem.* **2010**, *55* (14), 2089–2127. https://doi.org/10.1134/S0036023610140019.

(39) Dou, D.; Mavunkal, I. J.; Bauer, J. A. K.; Knobler, C. B.; Hawthorne, M. F.; Shore, S. G. Synthesis and Structure of Triethylammonium 2-(Acetonitrile)Nonahydro-Closo-Decaborate(1-). *Inorg. Chem.* **1994**, *33* (26), 6432–6434. https://doi.org/10.1021/ic00104a069.

(40) Matveev, E. Y.; Kubasov, A. S.; Razgonyaeva, G. A.; Polyakova, I. N.; Zhizhin, K. Y.; Kuznetsov, N. T. Reactions of the [B10H10]2− Anion with Nucleophiles in the Presence of Halides of Group IIIA and IVB Elements. *Russ. J. Inorg. Chem.* **2015**, *60* (7), 776–785. https://doi.org/10.1134/S0036023615070104.

(41) Zhdanov, A. P.; Klyukin, I. N.; Bykov, A. Y.; Grigoriev, M. S.; Zhizhin, K. Y.; Kuznetsov, N. T. Nucleophilic Addition of Alcohols to Anionic [2-B10H9NCR]−(R = Et, t-Bu): An Approach to Producing New Borylated Imidates. *Polyhedron* **2017**, *123*, 176–183. https://doi.org/10.1016/j.poly.2016.11.035.

(42) Daines, E. A.; Bolotin, D. S.; Bokach, N. A.; Gurzhiy, V. V.; Zhdanov, A. P.; Zhizhin, K. Y.; Kuznetsov, N. T. Push-Pull Alkenes Bearing Closo-Decaborate Cluster Generated via Nucleophilic Addition of Carbanions to Borylated Nitrilium Salts. *Inorganica Chim. Acta* **2018**, *471*, 372–376. https://doi.org/10.1016/j.ica.2017.11.054.

(43) Abi-Ghaida, F.; Laila, Z.; Ibrahim, G.; Naoufal, D.; Mehdi, A. New Triethoxysilylated 10-Vertex Closo-Decaborate Clusters. Synthesis and Controlled Immobilization into Mesoporous Silica. *Dalt. Trans.* **2014**, *43* (34), 13087–13095. https://doi.org/10.1039/c4dt00772g.

(44) Abi-Ghaida, F.; Clément, S.; Safa, A.; Naoufal, D.; Mehdi, A. Multifunctional Silica Nanoparticles Modified via Silylated-Decaborate Precursors. *J. Nanomater.* **2015**, *2015*, 1–8. https://doi.org/10.1155/2015/608432.

(45) Axtell, J. C.; Saleh, L. M. A.; Qian, E. A.; Wixtrom, A. I.; Spokoyny, A. M. Synthesis and Applications of Perfunctionalized Boron Clusters. *Inorg. Chem.* **2018**, *57* (5), 2333–2350. https://doi.org/10.1021/acs.inorgchem.7b02912.

(46) Avnir, D.; Klein, L. C.; Levy, D.; Schubert, U.; Wojcik, A. B. Organo-Silica Sol-Gel Materials. In *PATAI'S Chemistry of Functional Groups*; John Wiley & Sons, Ltd: Chichester, UK, 2009. https://doi.org/10.1002/9780470682531.pat0202.

(47) Yorov, K. E.; Kottsov, S. Y.; Baranchikov, A. E.; Boytsova, O. V.; Kiskin, M. A.; Varaksina, E. A.; Kopitsa, G. P.; Lermontov, S. A.; Sidorov, A. A.; Pipich, V.; Len, A.; Agafonov, A. V.; Ivanov, V. K. Photoluminescent Porous Aerogel Monoliths Containing ZnEu-Complex: The First Example of Aerogel Modified with a Heteronuclear Metal Complex. *J. Sol-Gel Sci. Technol.* **2019**, *92* (2), 304–318. https://doi.org/10.1007/s10971-019-04958-9.

(48) Hawthorne, M. F.; Pitochelli, A. R. The Reactions of Bis-Acetonitrile Decaborane with Amines. *J. Am. Chem. Soc.* **1959**, *81* (20), 5519. https://doi.org/10.1021/ja01529a077.

(49) Zhdanov, A. P.; Nelyubin, A. V.; Klyukin, I. N.; Selivanov, N. A.; Bortnikov, E. O.; Grigoriev, M. S.; Zhizhin, K. Y.; Kuznetsov, N. T. Nucleophilic Addition Reaction of Secondary Amines to Acetonitrilium Closo-Decaborate [2-B10H9NCCH3]–. *Russ. J. Inorg. Chem.* **2019**, *64* (7), 841–846. https://doi.org/10.1134/S0036023619070180.

(50) Williams, D. B. G.; Lawton, M. Drying of Organic Solvents: Quantitative Evaluation of the Efficiency of Several Desiccants. *J. Org. Chem.* **2010**, *75* (24), 8351–8354. https://doi.org/10.1021/jo101589h.

(51) *Neutron activation and scattering calculator*.

(52) Han, B.; Popov, A. L.; Shekunova, T. O.; Kozlov, D. A.; Ivanova, O. S.; Rumyantsev, A. A.; Shcherbakov, A. B.; Popova, N. R.; Baranchikov, A. E.; Ivanov, V. K. Highly Crystalline WO 3 Nanoparticles Are Nontoxic to Stem Cells and Cancer Cells. *J. Nanomater.* **2019**, *2019*, 1–13. https://doi.org/10.1155/2019/5384132.

(53) Nelyubin, A. V.; Selivanov, N. A.; Bykov, A. Y.; Klyukin, I. N.; Novikov, A. S.; Zhdanov, A. P.; Karpechenko, N. Y.; Grigoriev, M. S.; Zhizhin, K. Y.; Kuznetsov, N. T. Primary Amine Nucleophilic Addition to Nitrilium Closo-Dodecaborate [B12H11NCCH3]−: A Simple and Effective Route to the New BNCT Drug Design. *Int. J. Mol. Sci.* **2021**, *22* (24), 13391. https://doi.org/10.3390/ijms222413391.

(54) Ezhov, A. V.; Vyal'ba, F. Y.; Kluykin, I. N.; Zhdanova, K. A.; Bragina, N. A.; Zhdanov, A. P.; Zhizhin, K. Y.; Mironov, A. F.; Kuznetsov, N. T. Synthesis of New Bioinorganic Systems Based on Nitrilium Derivatives of Closo-Decaborate Anion and Meso-Arylporphyrins with Pendant Amino Groups. *Macroheterocycles* **2017**, *10* (4–5), 505–509. https://doi.org/10.6060/mhc171254z.

(55) Šícha, V.; Plešek, J.; Kvíčalová, M.; Císařová, I.; Grüner, B. Boron(8) Substituted Nitrilium and Ammonium Derivatives, Versatile Cobalt Bis(1,2-Dicarbollide) Building Blocks for Synthetic Purposes. *Dalt. Trans.* **2009**, No. 5, 851–860. https://doi.org/10.1039/B814941K.

(56) Klyukin, I. N.; Selivanov, N. A.; Bykov, A. Y.; Zhdanov, A. P.; Zhizhin, K. Y.; Kuznetsov, N. T. Synthesis and Physicochemical Properties of C-Borylated Amides Based on the Closo-Decaborate Anion. *Russ. J. Inorg. Chem.* **2019**, *64* (11), 1405–1409. https://doi.org/10.1134/S0036023619110081.

(57) Klyukin, I. N.; Selivanov, N. A.; Bykov, A. Y.; Zhdanov, A. P.; Zhizhin, K. Y.; Kuznetsov, N. T. Synthesis and Physicochemical Properties of C-Borylated Esters and Amides Based on the Closo-Dodecaborate Anion. *Russ. J. Inorg. Chem.* **2020**, *65* (11), 1637–1641. https://doi.org/10.1134/S0036023620110091.

(58) Zhdanov, A. P.; Polyakova, I. N.; Razgonyaeva, G. A.; Zhizhin, K. Y.; Kuznetsov, N. T. Reactions of Nucleophilic Addition of Primary Amines to the Nitrilium Derivative of the Closo-Decaborate Anion [2-B10H9(N≡CCH3)]−. *Russ. J. Inorg. Chem.* **2011**, *56* (6), 847–855. https://doi.org/10.1134/S003602361106026X.

(59) Shi, F.; Wang, L.; Liu, J. Synthesis and Characterization of Silica Aerogels by a Novel Fast Ambient Pressure Drying Process. *Mater. Lett.* **2006**, *60* (29–30), 3718–3722. https://doi.org/10.1016/j.matlet.2006.03.095.

(60) Scherdel, C.; Reichenauer, G. Highly Porous Silica Xerogels without Surface Modification. *J. Supercrit. Fluids* **2015**, *106*, 160–166. https://doi.org/10.1016/j.supflu.2015.08.016.

(61) Thommes, M.; Kaneko, K.; Neimark, A. V.; Olivier, J. P.; Rodriguez-Reinoso, F.; Rouquerol, J.; Sing, K. S. W. Physisorption of Gases, with Special Reference to the Evaluation of Surface Area and Pore Size Distribution (IUPAC Technical Report). *Pure Appl. Chem.* **2015**, *87* (9–10), 1051–1069. https://doi.org/10.1515/pac-2014-1117.

(62) Stan, C. S.; Marcotte, N.; Secula, M. S.; Popa, M. A New Photoluminescent Silica Aerogel Based on N-Hydroxysuccinimide-Tb(III) Complex. *J. Sol-Gel Sci. Technol.* **2014**, *69* (1), 207–213. https://doi.org/10.1007/s10971-013-3205-4.

(63) Abdulrahman, S. T.; Ahmad, Z.; Thomas, S.; Rahman, A. A. Introduction to Neutron-Shielding Materials. In *Micro and Nanostructured Composite Materials for Neutron Shielding Applications*; Elsevier, 2020; pp 1–23. https://doi.org/10.1016/B978-0-12-819459-1.00001-5.

(64) Gwaily, S. .; Hassan, H. .; Badawy, M. .; Madani, M. Natural Rubber Composites as Thermal Neutron Radiation Shields. *Polym. Test.* **2002**, *21* (5), 513–517. https://doi.org/10.1016/S0142-9418(01)00117-9.

(65) Radiation Shielding Members Including Nano-Particles Asa Radation Shielding Materal and Method for Preparing the Same. US 2010/0102279 A1.

(66) Adeli, R.; Shirmardi, S. P.; Ahmadi, S. J. Neutron Irradiation Tests on B4C/Epoxy Composite for Neutron Shielding Application and the Parameters Assay. *Radiat. Phys. Chem.* **2016**, *127*, 140–146. https://doi.org/10.1016/j.radphyschem.2016.06.026.

(67) Özdemir, T.; Akbay, İ. K.; Uzun, H.; Reyhancan, İ. A. Neutron Shielding of EPDM Rubber with Boric Acid: Mechanical, Thermal Properties and Neutron Absorption Tests. *Prog. Nucl. Energy* **2016**, *89*, 102–109. https://doi.org/10.1016/j.pnucene.2016.02.007.

(68) Özdemir, T.; Güngör, A.; Reyhancan, İ. A. Flexible Neutron Shielding Composite Material of EPDM Rubber with Boron Trioxide: Mechanical, Thermal Investigations and Neutron

Shielding Tests. *Radiat. Phys. Chem.* **2017**, *131*, 7–12. https://doi.org/10.1016/j.radphyschem.2016.10.012.

(69) Abdel-Aziz, M. M.; Gwaily, S. E.; Makarious, A. S.; El-Sayed Abdo, A. Ethylene-Propylene Diene Rubber/Low Density Polyethylene/Boron Carbide Composites as Neutron Shields. *Polym. Degrad. Stab.* **1995**, *50* (2), 235–240. https://doi.org/10.1016/0141-3910(95)00177-8.